

Constraining the mass of the Local Group

Edoardo Carlesi,¹ * Yehuda Hoffman,¹ Jenny G. Sorce,² Stefan Gottlöber²

¹*Racah Institute of Physics, Givat Ram, 91040 Jerusalem, Israel*

²*Leibniz-Institut für Astrophysik Potsdam (AIP), An der Sternwarte 16, D-14482 Potsdam, Germany*

Submitted XXXX May XXXX

ABSTRACT

The mass of the Local Group (LG) is a crucial parameter for galaxy formation theories. However, its observational determination is challenging - its mass budget is dominated by dark matter which cannot be directly observed. To meet this end the posterior distributions of the LG and its massive constituents have been constructed by means of constrained and random cosmological simulations. Two priors are assumed - the Λ CDM model that is used to set up the simulations and a LG model, which encodes the observational knowledge of the LG and is used to select LG-like objects from the simulations. The constrained simulations are designed to reproduce the local cosmography as it is imprinted onto the Cosmicflows-2 database of velocities. Several prescriptions are used to define the LG model, focusing in particular on different recent estimates of the tangential velocity of M31. It is found that (a) different v_{tan} choices affect the peak mass values up to a factor of 2, and change mass ratios of M_{M31} to M_{MW} by up to 20%; (b) constrained simulations yield more sharply peaked posterior distributions compared with the random ones; (c) LG mass estimates are found to be smaller than those found using the timing argument; (d) preferred MW masses lie in the range of $(0.6 - 0.8) \times 10^{12} M_{\odot}$ whereas (e) M_{M31} is found to vary between $(1.0 - 2.0) \times 10^{12} M_{\odot}$, with a strong dependence on the v_{tan} values used.

Key words: Cosmology, Numerical simulations, Dark matter, Local Group

1 INTRODUCTION

The impressive developments of cosmology of the past few years have been driven by a remarkable improvement in the quality and quantity of available data as well as a substantial effort in the theoretical and numerical modeling devoted at accommodating them within a single, coherent framework, that is the standard Λ Cold Dark Matter model (Λ CDM). Thanks to the advancements in the numerical simulation techniques it has become possible to simulate objects of the size of our Local Group (LG) of galaxies, allowing to test both standard (e.g. Boylan-Kolchin et al. 2012; Zavala et al. 2012; Garrison-Kimmel et al. 2014; Tollerud et al. 2014) and alternative cosmological theories on small scales (e.g. Elahi et al. 2015; Penzo et al. 2016; Garaldi et al. 2016). This is the subject of near field cosmology, whose purpose is to extract cosmologically-relevant information from the high-quality observations of the nearby universe.

However, estimating the abundance of dark matter (DM) in the immediate neighbourhood is still challenging. In particular, the exact size of the two halos hosting the Milky Way (MW) and Andromeda (M31) galaxies is known only within a large degree of uncertainty. Viral mass estimates for the DM haloes of both M31 and MW are still just loosely constrained by observations (Kochanek 1996; Wilkinson & Evans 1999; Evans & Wilkinson 2000; van

der Marel & Guhathakurta 2008; Karachentsev et al. 2009; van der Marel et al. 2012; Gibbons et al. 2014) and in general need a substantial degree of modelling and theory to be inferred (see e.g. Peebles et al. 2001; Li & White 2008; McMillan 2011; Fardal et al. 2013; Boylan-Kolchin et al. 2013; Diaz et al. 2014; Cautun et al. 2014; Wang et al. 2015).

A popular and straightforward way of addressing the problem is represented by the “timing argument” (TA, Kahn & Woltjer 1959) which models the LG halo pair as point-like particles that depart from each other after the Big Bang while decelerating under their own gravity, until they start approaching. Although simple and insightful, this simple analytical approach can be improved by further modeling including elements such as dark energy (Partridge et al. 2013) or the Large Magellanic Cloud (Peñarrubia et al. 2016).

Cosmological N -body simulations, on the other hand, provide an alternative tool to study the mass of the LG and its members (Busha et al. 2011; González et al. 2014). However, they require a prior knowledge of the cosmological model and the objects under investigation. This means that, in general, a suitable *Local Group Model*, a set of prior that incorporates our previous knowledge of the system, has to be introduced and specified.

In this *Paper* we address the issue of determining the total mass of the local group M_{LG} and its main components following the method described in Carlesi et al. (2016b) to derive posterior distribution functions for the tangential velocity of M31 using a simple LG model. This kind of Bayesian approach is in turn simi-

* E-mail: carlesi@phys.huji.ac.il

lar to the what Busha et al. (2011) used to constrain M_{MW} and to that of González et al. (2014) for the M_{LG} . In the present work, most of the emphasis is put on the consequences that the different v_{tan} estimates of Sohn et al. (2012) and Salomon et al. (2016) (referred to as $v_{\text{tan}}^{(I)}$ and $v_{\text{tan}}^{(II)}$ hereafter) have on the mass of the Local Group of galaxies, and on the masses of the two largest DM haloes, M31 and MW. In fact, whereas the first authors directly measured an extremely small value of v_{tan} , compatible with zero at the 1σ level, the latter found that new satellite data favour a much higher $v_{\text{tan}} \approx 160 \text{ km s}^{-1}$. Each one of these values is expected to have substantially different implications for the mass of the LG and its members, which are going to be discussed here.

Moreover, two different halo samples are used. The first one comes from the so called Local Group Factory simulation series introduced by Carlesi et al. (2016a), and provides a large number of LG-like objects within a large scale environment quantitatively and qualitatively close to the real one. Here, the Cosmicflows 2 (CF2, Tully et al. 2013) dataset is used to generate the initial conditions, constraining the variance of the simulations and thus shaping the $z = 0$ properties of the LG neighbourhood. The second one is a control sample drawn from a standard (random) ΛCDM simulation. The comparison between the results obtained within the two samples will allow to highlight the influence of the particular environment on M_{LG} , M_{M31} and M_{MW} , and disentangle it from the effect of the kinematic priors used to define LGs.

This work is structured as follows. Section 2 contains a description of the simulations and the methods used, with particular emphasis on the choice of the priors used to derive a posterior distribution functions. Section 3 describes these result for M_{LG} , M_{M31} , M_{MW} and their ratio under different choices of the priors, highlighting the influence of v_{tan} on the final estimates and also comparing the results to the values provided by other authors. In Section 4 we summarize our main results and discuss their implications.

2 METHODS

In this section we review the methods and the simulations used to derive the posterior likelihood functions, as already discussed by Carlesi et al. (2016b).

2.1 The Simulations

LG-like halo pairs are drawn from two classes of ΛCDM simulations running with Planck-I cosmological parameters $\Omega_m = 0.31$, $\Omega_\Lambda = 0.69$, $h = 0.67$ and $\sigma_8 = 0.83$ (Planck Collaboration 2014). DM halo catalogues are produced using the AHF halo finder (Knollmann & Knebe 2009); halo masses are defined by M_{200} with respect to ρ_{crit} . Total LG mass is simply defined as $M_{\text{LG}} = M_{\text{MW}} + M_{\text{M31}}$. The first LG sample is generated by selecting pairs out of 700 Constrained Simulations (CSs), obtained using the Local Group factory numerical pipeline (Carlesi et al. 2016a). It has been shown that these candidates live by construction in a large scale environment akin to the observational one, starting from suitable Initial Conditions (ICs) (Doumler et al. 2013a,b,c; Sorce et al. 2014, 2016) generated using (grouped) CF2 peculiar velocity data (Tully et al. 2013) as constraints; biases have been minimized using the method of Sorce (2015). The standard random realization of the ΛCDM model, from which the second sample (labeled

Table 1. Kinematic priors on velocities (in km/s) and relative distances of the haloes (in $h^{-1} \text{ Mpc}$). The first (last) three choices feature $\pm 25\%$ ($\pm 50\%$) intervals around the r and v_{tan} values of van der Marel et al. (2012). Mod1 features no v_{tan} restriction, for Mod2 and Mod4 $v_{\text{tan}}^{(I)} \pm 1\sigma$ have been chosen while Mod3 and Mod6 use $v_{\text{tan}}^{(II)} \pm 1\sigma$ priors.

	V_{rad}	V_{tan}	r
Mod1	$[-135, -80]$	—	$[0.35, 0.70]$
Mod2	$[-135, -80]$	$[0, 34]$	$[0.35, 0.70]$
Mod3	$[-135, -80]$	$[103, 225]$	$[0.35, 0.70]$
Mod4	$[-150, -55]$	—	$[0.25, 0.78]$
Mod5	$[-150, -55]$	$[0, 34]$	$[0.25, 0.78]$
Mod6	$[-150, -55]$	$[103, 225]$	$[0.25, 0.78]$

Rand) was drawn, has been provided by the CurieHZ project¹, and consists of a single DM simulation with 1024^3 particles within a $200h^{-1} \text{ Mpc}$ box. The mass resolution in both CS and Rand simulation is $6.5 \times 10^8 h^{-1} M_\odot$, which allows to resolve haloes of mass $\sim 10^{12} h^{-1} M_\odot$ with ~ 200 DM particles. Thanks to the fact that both simulation types have the same DM particle mass, it is possible to factor out numerical effects when comparing the results between them.

2.2 The Local Group Model

Before discussing the properties of LG-like objects, it is obviously necessary to specify the set of properties used to identify it. This is what we call here *Local Group model* - in different contexts (e.g. hydrodynamical simulations) different models can be invoked. Any choice of the Local Group Model reflects our prior observational knowledge on the system considered. Following the observation that the LG system is dominated by a pair of spiral galaxies, the MW and M31, simulated LGs are first of all defined as a pair of DM haloes.

M31 (MW) is assumed to be the most (least) massive of the two, as suggested by a host of different considerations such as the measure of the tidal force acting on the MW (Baiesi Pillastrini 2009), the position of the barycenter of the LG given by the local Hubble flow (Karachentsev et al. 2009) and the balance of the total angular momentum at the center of mass (Díaz et al. 2014). On the other hand, it has to be noticed that older results based on the dynamics of M31 dwarf spheroidal companions (e.g. Evans & Wilkinson 2000; Gottesman et al. 2002) have been pointing to an opposite direction. Therefore, it needs to be stressed that the choice $M_{\text{M31}} > M_{\text{MW}}$ is one of the assumptions of this particular Local Group model, and is not meant to suggest that the ratio of M31 to MW mass ratio is a settled issue.

Since the goal is to derive a posterior distribution function for M_{LG} , M_{M31} and M_{MW} , all observational inputs on the masses will be neglected. The focus will be thus placed on the kinematic properties of the pair: their tangential (v_{tan}) and radial (v_{rad}) velocities as well as inter-halo separation r . Moreover, even though observations on larger scales (such as the coldness of the local Hubble flow, (González et al. 2014), or the filamentary nature of our immediate neighbourhood (Libeskind et al. 2015)) have been shown to affect LG properties, environmental considerations are intentionally neglected in our model. In this way, it will be possible to single out

¹ <http://curiehz.ft.uam.es/>

the effects of the LG environment, which is by construction reproduced for all of the candidates drawn from the CS sample. The only external condition which all of the pairs are subjected to is *isolation*, meaning that no other object at least as massive as the lightest of the pair must reside within $2.5h^{-1}$ Mpc from the LG center of mass.

The ranges of allowed values for r , v_{rad} and v_{tan} are shown in Table 1. A set of six different priors has been used to define separate samples of LG like objects, using two different prescriptions for r and v_{rad} , which are very well known quantities, and v_{tan} . In the case of the latter, in fact, there is yet no clear consensus on its real value, for which currently two incompatible estimates exist. These were obtained using different techniques: the one of Sohn et al. (2012), who found $v_{\text{tan}} = 17 \pm 17$ (referred to as $v_{\text{tan}}^{(I)}$) directly measuring the motion stellar population within M31 against background galaxies; and the one of Salomon et al. (2016), who inferred $v_{\text{tan}} = 164 \pm 62$ (referred to as $v_{\text{tan}}^{(II)}$) using precise satellite galaxies data of the PAndAS survey (McConnachie et al. 2009; Martin et al. 2013a,b).

Due to the small $1 - \sigma$ errors around r and v_{rad} , in order to gather a statistically meaningful sample of LGs with properties reasonably close to the observational ones, we took intervals of $\pm 25\%$ and $\pm 50\%$ of the fiducial values taken from van der Marel et al. (2012). On the other hand, given the large uncertainties surrounding v_{tan} , $\pm 1\sigma$ priors have been used, to avoid being unnecessarily restrictive by imposing the same interval prescriptions of the other parameters. Given these choices, we proceed sampling the posterior distribution functions for M_{LG} , M_{M31} and M_{LG} from both Rand and CS simulations. LG-like pairs are searched for in the full box in the first case, while for each CF2-constrained simulation the search volume is limited to a $7h^{-1}$ Mpc sphere around the center of the box, to ensure that these pairs are living within an environment that reproduces the main features (such as Virgo, local filament and local void) of the observational one.

3 RESULTS

The six samples corresponding to the parameter combinations of Table 1 are used to derive numerical distributions for the masses which can be fitted by a log-normal function (as Busha et al. (2011) already noted for M_{MW}):

$$f(\log_{10}(M_{200}/M_{\odot})) = \frac{1}{\sqrt{2\pi}\sigma} \exp - \frac{(\log_{10}(M_{200}/M_{\odot}) - \mu)^2}{2\sigma^2} \quad (1)$$

The numerical means and standard deviations for the six combinations of the priors are shown in Table 2 for the \log_{10} values of the masses in M_{\odot} units; while Fig. 1 shows the distributions obtained for the first three sets of parameters. For each LG candidate we also compute the mass ratio of the larger to the smaller halo of the pair, i.e. $M_{\text{M31}}/M_{\text{MW}}$ in our convention, and in Table 3 we provide median, upper and lower quartile values of their distribution for each prior set. These values can be compared to those shown in Appendix A, which shows a large set of estimates of M_{LG} , M_{MW} and M_{M31} obtained different techniques and under different assumptions.

First of all, it has to be noticed that the r and v_{rad} priors play a minor role in shaping the likelihood function, resulting in a slight reduction of the peak masses of M_{LG} , M_{MW} and M_{M31} using 50% intervals at each given v_{tan} prior. This finding is in agreement with González et al. (2014) and Carlesi et al. (2016b), who found a weak

dependence of the posterior distribution function on a given set of priors around the fiducial values of van der Marel et al. (2012) for r and v_{tan} . Therefore, the next subsections will deal only with the results obtained for the first three – more restrictive – prior sets, as our main conclusions will be left largely unaltered by changing them. We also notice, as a general trend, that CS distributions are characterized by a narrower distribution around the peaks, leading to smaller error estimates, despite the substantial reduction in the number of objects within the samples.

3.1 Total mass

A first look at M_{LG} shows that the choice of the v_{tan} prior plays a main role in shaping the posterior distribution function, as can be seen by looking at the values obtained for $v_{\text{tan}}^{(I)}$ and $v_{\text{tan}}^{(II)}$, the most extreme cases. In fact, while the former yields $M_{\text{LG}}^{\text{CS}} = 1.79^{+0.51}_{-0.52} \times 10^{12} M_{\odot}$, the application of the latter results in $M_{\text{LG}}^{\text{CS}} = 3.47^{+1.16}_{-0.83} \times 10^{12} M_{\odot}$, a value which is almost a factor of 2 larger and nicely overlaps with the number $M_{\text{LG}} = 3.6^{+3.0}_{-2.6} \times 10^{12} M_{\odot}$ quoted by McLeod et al. (2016) feeding the same kind of $v_{\text{tan}}^{(II)}$ priors to a machine learning algorithm.

This holds also in the case of the Rand sample, for which similar numerical values have been obtained. Both results suggest that the total LG should be smaller than those obtained using the TA (e.g. Li & White 2008; Partridge et al. 2013) and least action methods (Phelps et al. 2013), which generally predict $M_{\text{LG}} > 4 \times 10^{12} M_{\odot}$. This is most likely due to the approximations behind the TA, as it has been showed that neglecting both v_{tan} (Fattahi et al. 2016; McLeod et al. 2016) and large satellites (such as the Large Magellanic Clouds, see Peñarrubia et al. (2016)) lead to overestimate the value of M_{LG} .

The above mentioned M_{LG} values are well consistent with the recent findings of González et al. (2014) and Diaz et al. (2014), who both favour a total mass of $\approx 2.5 \times 10^{12} M_{\odot}$, very close to our Mod1 estimate (which makes no assumptions on v_{tan}) that gives $M_{\text{LG}}^{\text{CS}} = 2.57^{+0.87}_{-1.19} \times 10^{12}$.

So despite the large differences caused by the different tangential velocities, we cannot strongly favour or disfavour any among $v_{\text{tan}}^{(I)}$ or $v_{\text{tan}}^{(II)}$, as the aforementioned authors place its value between the two. This means that the *total* M_{LG} alone cannot yet provide strong evidence on the nature of v_{tan} , and knowledge of masses of the individual LG members is required.

We also note that using $v_{\text{tan}}^{(I)}$ priors (or no v_{tan} priors at all), CS mass estimates tend to be larger than Rand ones. This is consistent with the findings shown in Carlesi et al. (2016b), where it was argued that CS tend to favour higher v_{tan} s, which in turn would lead to higher mass estimates (see Fattahi et al. 2016). Nonetheless, at a first glance, this results seems to be at odds with González et al. (2014), who pointed out that the total mass of the LG should be decreasing as a consequence of the environmental constrains on the sample. However, it has to be emphasized that our choice of the priors on $v_{\text{tan}}^{(I)}$ is much more restrictive (1σ , $v_{\text{tan}} < 34 \text{ km s}^{-1}$) compared to theirs (3σ , $v_{\text{tan}} < 68 \text{ km s}^{-1}$). Repeating the analysis using their same prior prescription we found $M_{\text{LG}}^{\text{CS}} = 2.12^{+0.43}_{-0.40} \times 10^{12} M_{\odot}$ and $M_{\text{LG}}^{\text{Rand}} = 2.26^{+0.40}_{-0.50} \times 10^{12} M_{\odot}$, in good qualitative agreement with their findings.

3.2 Individual masses

Our LG model defined M31 (MW) as the heaviest (lightest) halo of the pair, allowing us to inspect the properties of each member

Table 2. Median \pm 75th and 25th percentiles for the masses of the Milky Way, Andromeda and total mass in $10^{12}M_{\odot}$ units for both constrained and unconstrained simulations. μ and σ represent the the best fit values to a lognormal distribution. Each table shows an estimate given for a different set of priors on velocity (radial and tangential) and relative distance. The upper three tables implement intervals of $\pm 25\%$ around the fiducial values of v_{rad} and r while those for the lower three amount to $\pm 50\%$. For each table the number of CS and Rand pairs per prior choice is also shown.

Mod1, $N_{CS} = 857$, $N_{Rand} = 1004$				Mod2, $N_{CS} = 43$, $N_{Rand} = 252$			Mod3, $N_{CS} = 48$, $N_{Rand} = 174$		
	M_{200}	μ	σ	M_{200}	μ	σ	M_{200}	μ	σ
$M_{M31,CS}$	$1.77^{+0.72}_{-0.91}$	12.19	0.31	$1.07^{+0.31}_{-0.45}$	11.93	0.21	$2.48^{+0.80}_{-0.56}$	12.21	0.19
$M_{M31,Rand}$	$1.54^{+0.55}_{-0.80}$	12.14	0.31	$1.14^{+0.35}_{-0.46}$	12.00	0.25	$2.93^{+1.09}_{-1.57}$	12.33	0.29
$M_{MW,CS}$	$0.74^{+0.26}_{-0.41}$	11.80	0.30	$0.60^{+0.21}_{-0.14}$	11.69	0.19	$0.82^{+0.33}_{-0.68}$	11.76	0.35
$M_{MW,Rand}$	$0.66^{+0.28}_{-0.37}$	11.75	0.34	$0.47^{+0.16}_{-0.25}$	11.62	0.26	$1.06^{+0.60}_{-0.83}$	11.90	0.46
$M_{MLG,CS}$	$2.57^{+0.87}_{-1.19}$	12.38	0.27	$1.79^{+0.51}_{-0.51}$	12.20	0.14	$3.47^{+1.16}_{-0.83}$	12.41	0.16
$M_{MLG,Rand}$	$2.26^{+0.76}_{-1.14}$	12.30	0.27	$1.65^{+0.44}_{-0.66}$	12.15	0.20	$4.13^{+1.44}_{-2.11}$	12.52	0.27

Mod4, $N_{CS} = 1806$, $N_{Rand} = 4021$				Mod5, $N_{CS} = 160$, $N_{Rand} = 949$			Mod6, $N_{CS} = 125$, $N_{Rand} = 551$		
	M_{200}	μ	σ	M_{200}	μ	σ	M_{200}	μ	σ
$M_{M31,CS}$	$1.50^{+0.72}_{-0.95}$	12.11	0.38	$0.92^{+0.40}_{-0.48}$	11.93	0.31	$2.29^{+0.78}_{-1.04}$	12.28	0.28
$M_{M31,Rand}$	$1.26^{+0.60}_{-1.08}$	12.08	0.40	$0.81^{+0.34}_{-0.53}$	11.88	0.34	$3.00^{+1.18}_{-1.65}$	12.42	0.34
$M_{MW,CS}$	$0.58^{+0.24}_{-0.44}$	11.74	0.35	$0.46^{+0.19}_{-0.21}$	11.63	0.30	$0.79^{+0.35}_{-0.65}$	11.86	0.38
$M_{MW,Rand}$	$0.51^{+0.24}_{-0.45}$	11.69	0.40	$0.34^{+0.13}_{-0.26}$	11.53	0.31	$1.01^{+0.51}_{-0.97}$	11.96	0.42
$M_{MLG,CS}$	$2.21^{+0.95}_{-1.37}$	12.29	0.34	$1.36^{+0.54}_{-0.68}$	12.10	0.27	$3.40^{+1.29}_{-0.97}$	12.46	0.26
$M_{MLG,Rand}$	$1.84^{+0.82}_{-1.53}$	12.24	0.37	$1.20^{+0.49}_{-0.70}$	12.06	0.28	$4.14^{+1.58}_{-2.52}$	12.57	0.33

of the LG. Models of the kind $M_{MW} > M_{M31}$ are neglected in this work, though they cannot be excluded - as noticed earlier. In what follows, the main findings regarding M_{MW} and M_{M31} are presented along with their consistency with existing results found by other authors.

Andromeda Mod1 and Mod3 results for M_{M31} are in very good agreement with the value of $\log_{10}(M_{M31}) = 12.3 \pm 0.1$ derived by Fardal et al. (2013). Remarkably, although both CS and Rand values overlap with it within the scatter, best fit peak values for the former group of simulations are remarkably much closer. Indeed, if M31 turns out to be this massive, it would directly favour the $v_{\text{tan}}^{(II)}$ value over $v_{\text{tan}}^{(I)}$, in agreement with Fattahi et al. (2016) who pointed out that larger masses are in general associated with higher tangential velocities in cosmological simulations. On the other hand, it turns out the likelihood functions of M_{M31} derived with small tangential velocity LG-model (Mod2), show a well defined peak around a smaller mass, $M_{M31}^{CS} = 1.07^{+0.27}_{-0.50} \times 10^{12}M_{\odot}$. Such a light M31 would still be compatible with some of the older estimates (see e.g. Evans & Wilkinson 2000; Gottesman et al. 2002; Ibata et al. 2004), for v_{rad} and r , but is of course in conflict with the aforementioned - more recent - results, reminding us of the importance of a precise measurement of v_{tan} in order to obtain a complete and consistent picture of the LG.

Milky Way As a consequence of our initial assumption $M_{MW} < M_{M31}$, the MW is characterized by a small mass. This is true in particular in the CS case, for which $v_{\text{tan}}^{(I)}$ values yield $M_{MW,CS} = 0.60^{+0.21}_{-0.14} \times 10^{12}M_{\odot}$ and $M_{MW,CS} = 0.82^{+0.33}_{-0.68} \times 10^{12}M_{\odot}$ for $v_{\text{tan}}^{(II)}$. These numbers are both consistent with a large number of recent results (Bovy et al. 2012; Deason et al. 2012; Rashkov et al. 2013; Gibbons et al.

2014; Eadie et al. 2016) that indicate a MW mass in the range $(0.5 - 1.0) \times 10^{12}M_{\odot}$. On the other hand, they appear to be on the low end of the $1.26 \pm 0.24 \times 10^{12}M_{\odot}$ and $1.3 \pm 0.3 \times 10^{12}M_{\odot}$ values computed by McMillan (2011, 2016) modelling the mass distribution of the Galaxy, as well as the $1.2 - 1.7 \times 10^{12}M_{\odot}$ constraints of Fragione & Loeb (2016) obtained using ultra high velocity stars. Moreover, such a light mass would in turn disfavour a bound orbit for Leo I. This remark is consistent with the analysis made by Watkins et al. (2010) and Boylan-Kolchin et al. (2013), who showed that a bound Leo I alone would shift the M_{MW} estimate upwards by $\approx 30\%$. Therefore, removing it from the list of MW satellites, significantly smaller M_{MW} values can be obtained, leading to a good agreement with our results. On the other hand, an unbound Leo I at odds with what has been suggested by other authors, most notably Boylan-Kolchin et al. (2013), arguing in favour of a bound orbit based on N -body simulations. However, in order to consistently address the issue at the root of this discrepancy from the standpoint of CSs, it is necessary to use higher resolution simulations, which allow to deal with substructure with a sufficient level of accuracy; a subject which is currently being pursued.

Mass ratios Given the above results for the individual halo masses, it is possible to draw a few final conclusions regarding the *mass ratios* of the pair, which were shown in Table 3. The numerical values of these ratios show a good agreement with results obtained by Diaz et al. (2014), who derived a ratio of $2.3^{+2.1}_{-1.1}$ by enforcing the zero angular momentum condition with respect to the center of mass of the LG. Lower ratios, such as the one of $\approx 5/4$ derived by Karachentsev et al. (2009), seem to be slightly in tension with the present results, which favour ratios > 1.3 for both CS and Rand simulations at the 75% level. Thanks to the use

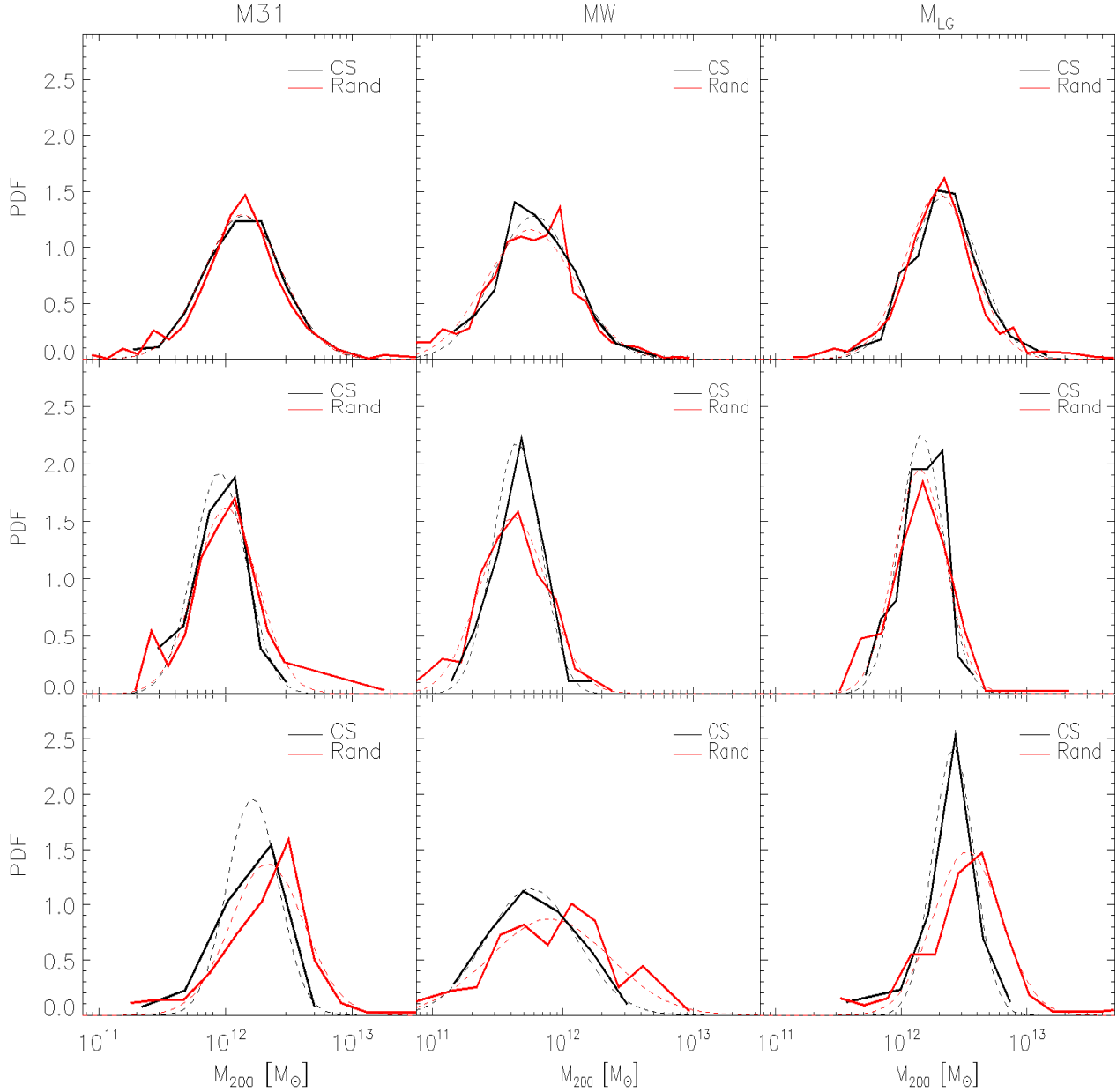


Figure 1. Probability distributions for the MW, M31 and LG masses. The figures on the first line show the results corresponding to Mod1, on the second line to Mod2 and the third one to Mod3. CS results are characterized by a reduced scatter around the peak likelihood values, as is particularly clear in the second and third lines in the case of M_{LG} distributions.

of different LG models and different halo samples it is possible to disentangle the influence that either of the two play in determining those ratios. We first remark that both CS and Rand LGs show the same qualitative behaviour under a change of v_{tan} priors: namely, the gap between MW and M31 masses is enhanced when switching from $v_{\text{tan}}^{(I)}$ to $v_{\text{tan}}^{(II)}$ constraints. In particular, this change is larger (shifting up to 25%, from 1.64 to 2.01) in the case of CS, as a consequence of the minor change of M_{MW} masses (from $0.6 \times 10^{12} M_{\odot}$ to $0.8 \times 10^{12} M_{\odot}$) with respect to M_{M31} , which increases from $\approx 1.0 \times 10^{12} M_{\odot}$ to $\approx 2.0 \times 10^{12} M_{\odot}$ with increasing v_{tan} . Ratios in the Rand sample, though affected in the same manner, appear less pronounced and are characterized by larger variability intervals; moreover, the median values of these ratios are always above the CS ones, overlapping at the confidence level of

the 25-th and 75-th percentiles. It is thus possible to conclude that v_{tan} values not only affect individual masses, but mass ratios as well, by affecting them unevenly.

4 CONCLUSIONS

We have derived the posterior probability distribution functions of the mass of the Local Group and its main constituents, the Milky Way and the M31 galaxies. These posterior distributions have been derived by means of constrained and random DM-only cosmological simulations. The prior assumptions that condition the above probability distributions are: a. The standard Λ CDM cosmological model; b. A Local Group model, which summarizes the observa-

Table 3. Median ratios M_{M31}/M_{MW} for the different LG models, within CS and Rand LG samples. Intervals are given by the 25-th and 75-th percentiles of the distributions. Lower v_{tan} values are correlated with smaller mass ratios in both CS and Rand. We also note that, for any given set of priors, CS samples predict smaller values of M_{M31} to M_{MW} with a reduced scatter around the median value.

Prior	CS	Rand
Mod1	$1.90^{+1.25}_{-0.58}$	$2.10^{+1.67}_{-0.70}$
Mod2	$1.64^{+0.61}_{-0.34}$	$2.03^{+1.16}_{-0.79}$
Mod3	$2.01^{+1.88}_{-0.66}$	$2.13^{+2.87}_{-0.89}$
Mod4	$1.90^{+1.43}_{-0.57}$	$2.09^{+1.79}_{-0.69}$
Mod5	$1.73^{+0.83}_{-0.40}$	$1.96^{+1.41}_{-0.58}$
Mod6	$2.13^{+1.66}_{-0.76}$	$2.28^{+2.19}_{-1.01}$

tional knowledge of the LG and thereby defines what a LG-like object is. The numerical simulations are the means by which the posterior distributions are constructed - the Λ CDM model is used to set up the simulations and the LG model is used to select LG-like objects. The Cosmicflows-2 database of peculiar velocity is setting another prior on the constrained simulations, which are designed to reproduce the imprint of the local universe on the CF2 data. The choice of the LG model and the CF2 constraint allows us to study the way the structure of the LG and the nearby universe affects our knowledge of masses of the MW and M31. A particular emphasis has been placed also on the effects of using a low- v_{tan} estimate (the value found by Sohn et al. (2012), referred to as $v_{\text{tan}}^{(I)}$) and a high one ($v_{\text{tan}}^{(II)}$, derived by Salomon et al. (2016)).

We applied these models to objects drawn from two different types of simulations: a series of constrained simulations (CS), from which it was possible to gather halo pairs living in a large scale environment akin to the observational one, and a standard, random Λ CDM (Rand). We derived posterior distribution functions for the mass of the Local Group (LG) and its most prominent members, MW and M31, using the cosmological model Λ CDM and different possible definitions for the LG itself. This setup was designed to address several questions:

- what are the implications of the different v_{tan} values for M_{LG} , M_{M31} and M_{MW} ?
- what is the role of the environment in shaping the posterior distribution functions?
- how do different priors on well measured quantities (v_{rad} and r) affect the predicted mass distribution?

After establishing that the particular choices for v_{rad} and r priors have only a minor effect on the results (in agreement with the findings of González et al. (2014); Carlesi et al. (2016b)), it has been possible to determine the following:

- (a) v_{tan} priors play a dominant role in shifting the peak of the likelihood for all the masses. In fact, estimates based on $v_{\text{tan}}^{(I)}$ and $v_{\text{tan}}^{(II)}$ differ up to more than a factor of 2.
- (b) CS estimates for masses and ratios are characterized by a $\approx 25\%$ less in the scatter around the median values compared to

Rand results.

- (c) M_{M31} to M_{MW} ratios are slightly but systematically lower in CSs than in their Rand counterparts. Moreover, they are more affected by the change in v_{tan} prior choice, with a $\approx 25\%$ difference between $v_{\text{tan}}^{(I)}$ and $v_{\text{tan}}^{(II)}$.

- (d) MW mass values derived from CS samples consistently point towards $M_{\text{MWs}} \approx (0.5 - 1.0) \times 10^{12} M_{\odot}$, in good agreement with the recent findings of Deason et al. (2012); Bovy et al. (2012); Rashkov et al. (2013); Gibbons et al. (2014), and lying on the lower end of the intervals provided by McMillan (2011); Fragione & Loeb (2016); McMillan (2016). This is largely independent of the choice of v_{tan} .

- (e) Peak likelihood masses for M31 in CS simulation (Mod1 and Mod3) are extremely close to the $\log_{10} M_{M31} = 12.3 \pm 0.1$ value Fardal et al. (2013), indicating that a higher v_{tan} value is in better agreement with those data. Rand results are also compatible within the errors with those estimated, though their peak likelihoods are not as close.

We also found that our M_{LG} estimates tend to be smaller than TA ones, in agreement with González et al. (2014); Fattahi et al. (2016)). This inconsistency cannot be explained by definitions of the mass alone (e.g. collapsed mass vs. M_{vir}) and is most likely due to the crude approximations of the method (Peñarrubia et al. 2016). On the other hand, the results we obtained for the masses significantly overlap with previous estimates obtained by other means, while at the same time providing more insight and singling out the effects of the environment and the implications of each different v_{tan} measure. Moreover, the scatter around the peaks for the mass likelihood functions turns out to be smaller as a consequence of the constrained variance, as opposed to the unconstrained results which display consistently higher σ s.

Future investigation along these lines will be based on a set of higher resolution Local Group Factory simulations, which will allow to study mass accretion histories and satellite populations. In particular, we plan to analyze the properties of substructure around MW and M31 analogues to clarify the effect of the farthest massive satellites on LG mass estimation and address the source of disagreement with the MW mass estimates of Busha et al. (2011) and Boylan-Kolchin et al. (2013), which were inferred by the properties of the Large Magellanic Cloud and Leo I, respectively.

To sum up, we have shown that our Bayesian analysis of the masses of the local group and its main members provides consistent results given a simple prior model (our LG model and Λ CDM) and CF2 data. Moreover, we have been able to derive useful formulas that can be generally used for analytical modelling of the LG masses.

ACKNOWLEDGEMENTS

EC would like to thank the Lady Davis Fellowship Fund for financial support. YH has been partially supported by the Israel Science Foundation (1013/12). JS acknowledges support from the Alexander von Humboldt foundation.

REFERENCES

- Baiesi Pillastrini G. C., 2009, *MNRAS*, 397, 1990
- Battaglia G., Helmi A., Morrison H., Harding P., Olszewski E. W., Mateo M., Freeman K. C., Norris J., Shectman S. A., 2005, *Mon. Not. Roy. Astron. Soc.*, 364, 433
- Bovy J., et al., 2012, *ApJ*, 759, 131
- Boylan-Kolchin M., Bullock J. S., Kaplinghat M., 2012, *MNRAS*, 422, 1203
- Boylan-Kolchin M., Bullock J. S., Sohn S. T., Besla G., van der Marel R. P., 2013, *ApJ*, 768, 140
- Busha M. T., Marshall P. J., Wechsler R. H., Klypin A., Primack J., 2011, *ApJ*, 743, 40
- Carlesi E., Hoffman Y., Sorce J. G., Gottlöber S., Yepes G., Courtois H., Tully R. B., 2016b, *MNRAS*, 460, L5
- Carlesi E., Sorce J. G., Hoffman Y., Gottlöber S., Yepes G., Libeskind N. I., Pilipenko S. V., Knebe A., Courtois H., Tully R. B., Steinmetz M., 2016a, *MNRAS*, 458, 900
- Cautun M., Frenk C. S., van de Weygaert R., Hellwing W. A., Jones B. J. T., 2014, *MNRAS*, 445, 2049
- Courteau S., van den Bergh S., 1999, *Astron. J.*, 118, 337
- Deason A. J., Belokurov V., Evans N. W., An J., 2012, *MNRAS*, 424, L44
- Deason A. J., Belokurov V., Evans N. W., Koposov S. E., Cooke R. J., Peñarrubia J., Laporte C. F. P., Fellhauer M., Walker M. G., Olszewski E. W., 2012, *MNRAS*, 425, 2840
- Dehnen W., McLaughlin D., Sachania J., 2006, *Mon. Not. Roy. Astron. Soc.*, 369, 1688
- Diaz J. D., Koposov S. E., Irwin M., Belokurov V., Evans N. W., 2014, *MNRAS*, 443, 1688
- Doumler T., Courtois H., Gottlöber S., Hoffman Y., 2013b, *MNRAS*, 430, 902
- Doumler T., Gottlöber S., Hoffman Y., Courtois H., 2013c, *MNRAS*, 430, 912
- Doumler T., Hoffman Y., Courtois H., Gottlöber S., 2013a, *MNRAS*, 430, 888
- Eadie G., Springford A., Harris W., 2016, *ArXiv* 1609.06304
- Elahi P. J., Lewis G. F., Power C., Carlesi E., Knebe A., 2015, *MNRAS*, 452, 1341
- Evans N. W., Wilkinson M. I., 2000, *MNRAS*, 316, 929
- Fardal M. A., Weinberg M. D., Babul A., Irwin M. J., Guhathakurta P., Gilbert K. M., Ferguson A. M. N., Ibata R. A., Lewis G. F., Tanvir N. R., Huxor A. P., 2013, *MNRAS*, 434, 2779
- Fattahi A., Navarro J. F., Sawala T., Frenk C. S., Oman K. A., Crain R. A., Furlong M., Schaller M., Schaye J., Theuns T., Jenkins A., 2016, *MNRAS*, 457, 844
- Fragione G., Loeb A., 2016, *ArXiv* 1608.01517
- Garaldi E., Baldi M., Moscardini L., 2016, *JCAP*, 1, 050
- Garrison-Kimmel S., Boylan-Kolchin M., Bullock J. S., Kirby E. N., 2014, *MNRAS*, 444, 222
- Gibbons S. L. J., Belokurov V., Evans N. W., 2014, *MNRAS*, 445, 3788
- Gnedin O. Y., Brown W. R., Geller M. J., Kenyon S. J., 2010, *Astrophys. J.*, 720, L108
- Gonzalez R. E., Kravtsov A. V., Gnedin N. Y., 2013, *Astrophys. J.*, 770, 96
- González R. E., Kravtsov A. V., Gnedin N. Y., 2014, *ApJ*, 793, 91
- Gottesman S. T., Hunter J. H., Boonyasait V., 2002, *MNRAS*, 337, 34
- Ibata R., Chapman S., Ferguson A. M. N., Irwin M., Lewis G., McConnachie A., 2004, *MNRAS*, 351, 117
- Kahn F. D., Woltjer L., 1959, *ApJ*, 130, 705
- Karachentsev I. D., Kashibadze O. G., Makarov D. I., Tully R. B., 2009, *MNRAS*, 393, 1265
- Klypin A., Zhao H., Somerville R. S., 2002, *ApJ*, 573, 597
- Knollmann S. R., Knebe A., 2009, *ApJS*, 182, 608
- Kochanek C. S., 1996, *ApJ*, 457, 228
- Li Y.-S., White S. D. M., 2008, *MNRAS*, 384, 1459
- Libeskind N. I., Tempel E., Hoffman Y., Tully R. B., Courtois H., 2015, *MNRAS*, 453, L108
- McLeod M., Libeskind N., Lahav O., Hoffman Y., 2016
- Martin N. F., et al., 2013a, *ApJ*, 772, 15
- Martin N. F., et al., 2013b, *ApJ*, 779, L10
- McConnachie A. W., et al., 2009, *Nature*, 461, 66
- McMillan P. J., 2011, *MNRAS*, 414, 2446
- McMillan P. J., 2016, *ArXiv* 1608.00971
- Partridge C., Lahav O., Hoffman Y., 2013, *MNRAS*, 436, L45
- Peñarrubia J., Fattahi A., 2016
- Peñarrubia J., Gómez F. A., Besla G., Erkal D., Ma Y.-Z., 2016, *MNRAS*, 456, L54
- Peebles P. J. E., Phelps S. D., Shaya E. J., Tully R. B., 2001, *ApJ*, 554, 104
- Penzo C., Macciò A. V., Baldi M., Casarini L., Oñorbe J., Dutton A. A., 2016, *MNRAS*, 461, 2490
- Phelps S., Nusser A., Desjacques V., 2013, *ApJ*, 775, 102
- Planck Collaboration 2014, *A&A*, 571, A16
- Rashkov V., Pillepich A., Deason A. J., Madau P., Rockosi C. M., Guedes J., Mayer L., 2013, *ApJ*, 773, L32
- Sakamoto T., Chiba M., Beers T. C., 2003, *Astron. Astrophys.*, 397, 899
- Salomon J.-B., Ibata R. A., Famaey B., Martin N. F., Lewis G. F., 2016, *MNRAS*, 456, 4432
- Smith M. C., et al., 2007, 379, 755
- Sohn S. T., Anderson J., van der Marel R. P., 2012, *ApJ*, 753, 7
- Sorce J. G., 2015, *MNRAS*, 450, 2644
- Sorce J. G., Courtois H. M., Gottlöber S., Hoffman Y., Tully R. B., 2014, *MNRAS*, 437, 3586
- Sorce J. G., Gottlöber S., Yepes G., Hoffman Y., Courtois H. M., Steinmetz M., Tully R. B., Pomarède D., Carlesi E., 2016, *MNRAS*, 455, 2078
- Tollerud E. J., Boylan-Kolchin M., Bullock J. S., 2014, *MNRAS*, 440, 3511
- Tollerud E. J., et al., 2012, *Astrophys. J.*, 752, 45
- Tully R. B., Courtois H. M., Dolphin A. E., Fisher J. R., Héraudeau P., Jacobs B. A., Karachentsev I. D., Makarov D., Makarova L., Mitronova S., Rizzi L., Shaya E. J., Sorce J. G., Wu P.-F., 2013, *AJ*, 146, 86
- van der Marel R. P., Fardal M., Besla G., Beaton R. L., Sohn S. T., Anderson J., Brown T., Guhathakurta P., 2012, *ApJ*, 753, 8
- van der Marel R. P., Guhathakurta P., 2008, *ApJ*, 678, 187
- Wang W., Han J., Cooper A. P., Cole S., Frenk C., Lowing B., 2015, *MNRAS*, 453, 377
- Watkins L. L., Evans N. W., An J. H., 2010, *MNRAS*, 406, 264
- Wilkinson M. I., Evans N. W., 1999, *Mon. Not. Roy. Astron. Soc.*, 310, 645
- Xue X. X., et al., 2008, *The Astrophysical Journal*, 684, 1143
- Zaritsky D., Courtois H., 2016, *ArXiv e-prints* 1611.04574
- Zavala J., Avila-Reese V., Firmani C., Boylan-Kolchin M., 2012, *MNRAS*, 427, 1503

This paper has been typeset from a \LaTeX file prepared by the author.

APPENDIX A: LOCAL GROUP MASSES

In this appendix we provide a summary of some different estimates of M_{MW} (shown in Table A1), M_{M31} (Table A2) and M_{LG} (Table A3). These tables contain mostly those values which have been quoted throughout this work and is provided as a quick reference for the reader to the vast amount of results obtained using a large number of techniques. Due to the huge number of works that can be found in the literature on the subject, these tables are not meant to be exhaustive accounts of all the results, but rather present a broad overview of the variety of the methods used and values that have been obtained. For some authors more than one value is quoted when different assumptions were used within the same publication.

Table A1. Milky Way mass estimates in $10^{12}M_{\odot}$ units.

M_{MW}			
Source	Type of mass	Value	Method
Kochanek (1996)	$M(100\text{kpc})$	0.54 ± 0.13	Satellites & stars escape velocity
Kochanek (1996)	$M(100\text{kpc})$	$0.33 - 0.61$	Satellites & stars escape velocity incl. Leo I
Wilkinson & Evans (1999)	M_{vir}	$1.9^{+3.6}_{-1.7}$	Satellites & globular clusters
Klypin et al. (2002)	M_{vir}	$1.0 - 2.0$	Cuspy halo, adiabatic contraction
Sakamoto et al. (2003)	M_{vir}	$2.5^{+0.5}_{-1.0}$	Satellites (incl. Leo I)
Sakamoto et al. (2003)	M_{vir}	$1.8^{+0.0}_{-0.7}$	Satellites (excl. Leo I)
Battaglia et al. (2005)	M_{vir}	$0.8^{+1.2}_{-0.2}$	Radial velocity dispersion & NFW profile
Battaglia et al. (2005)	M_{vir}	$1.2^{+1.8}_{-0.5}$	Radial velocity dispersion & Truncated flat profile
Dehnen et al. (2006)	M_{vir}	≈ 1.5	Radial velocity dispersion
Smith et al. (2007)	M_{vir}	$1.42^{+1.14}_{-0.54}$	Local galactic escape speed
Xue et al. (2008)	M_{vir}	$1.0^{+0.3}_{-0.2}$	Line-of-sight velocity distribution
Li & White (2008)	M_{200}	$2.43^{+0.60}_{-0.73}$	TA calibrated on simulations
Gnedin et al. (2010)	$M(< 80\text{kpc})$	$0.69^{+0.30}_{-0.12}$	Halo stars radial velocities
McMillan (2011)	M_{vir}	1.26 ± 0.24	Satellites & radial DM distribution models
Busha et al. (2011)	M_{vir}	$1.2^{+0.7}_{-0.4}$	Large Magellanic clouds motion
Bovy et al. (2012)	M_{vir}	≈ 0.8	Rotation curve
Deason et al. (2012)	$M(< 50\text{kpc})$	≈ 0.4	Blue horizontal branch star kinematics
Deason et al. (2012)	$M(< 150\text{kpc})$	$(0.5 - 1.0)$	Radial velocities of stellar halo
Boylan-Kolchin et al. (2013)	M_{vir}	$1.6^{+0.8}_{-0.6}$	Leo I motion
Rashkov et al. (2013)	M_{vir}	≈ 0.8	SDSS halo stars & numerical simulations
Gonzalez et al. (2013)	M_{200}	$1.14^{+1.19}_{-0.41}$	Large Magellanic clouds properties
Gibbons et al. (2014)	$M(< 200\text{kpc})$	0.56 ± 0.12	Sagittarius stream
Diaz et al. (2014)	M_{vir}	0.8 ± 0.5	Momentum balance at the LG center of mass
Cautun et al. (2014)	M_{200}	$0.25 - 1.4$	Maximum circular velocity of satellites
McMillan (2016)	M_{vir}	1.30 ± 0.30	Satellites & radial DM distribution models & gas discs
Fragione & Loeb (2016)	M_{vir}	$1.2 - 1.7$	Hypervelocity stars
Eadie et al. (2016)	$M(< 179\text{kpc})$	$0.56 - 0.67$	Bayesian analysis of globular clusters
Peñarrubia et al. (2016)	M_{vir}	$1.04^{+0.26}_{-0.23}$	TA & Large Magellanic Clouds corrections
Peñarrubia & Fattahi (2016)	M_{vir}	≈ 0.85	Spherical collapse model & local Hubble flow
Zaritsky & Courtois (2016)	M_{vir}	> 0.77	Universal baryon fraction
Present paper	M_{200}	$0.60^{+0.21}_{-0.14}$	CS & $v_{\text{tan}}^{(I)}$
Present paper	M_{200}	$0.82^{+0.33}_{-0.68}$	CS & $v_{\text{tan}}^{(II)}$

Table A2. Andromeda mass estimates in $10^{12}M_{\odot}$ units.

M_{M31}			
Source	Type of mass	Value	Method
Evans & Wilkinson (2000)	M_{vir}	$1.23^{+1.8}_{-0.6}$	Satellites
Klypin et al. (2002)	M_{vir}	$1 - 2$	Cuspy halo model & adiabatic contraction
Gottesman et al. (2002)	$M(< 350\text{kpc})$	< 0.6	Dwarf satellites kinematics
Ibata et al. (2004)	$M(< 125\text{kpc})$	$0.75^{+0.25}_{-0.13}$	Giant stream kinematics
Watkins et al. (2010)	$M(< 300\text{kpc})$	1.40 ± 0.43	Satellites
Tollerud et al. (2012)	M_{vir}	$1.2^{+0.9}_{-0.7}$	Satellites
Fardal et al. (2013)	M_{200}	$1.99^{+0.51}_{-0.41}$	Giant stream kinematics
Diaz et al. (2014)	M_{vir}	1.7 ± 0.3	Momentum balance at the LG center of mass
Peñarrubia et al. (2016)	M_{vir}	$1.33^{+0.39}_{-0.33}$	TA & Large Magellanic Clouds corrections
Present paper	M_{200}	$1.07^{+0.31}_{-0.45}$	CS & $v_{\text{tan}}^{(I)}$
Present paper	M_{200}	$2.48^{+0.80}_{-0.56}$	CS & $v_{\text{tan}}^{(II)}$

Table A3. Local Group mass estimates in $10^{12}M_{\odot}$ units.

M_{LG}			
Source	Type of mass	Value	Method
Courteau & van den Bergh (1999)	$M(< 1.18\text{Mpc})$	2.3 ± 0.6	Velocity dispersion
Li & White (2008)	M_{200}	$5.27^{+0.93}_{-1.91}$	TA calibrated on simulations
van der Marel & Guhathakurta (2008)	M_{vir}	$5.58^{+0.85}_{-0.72}$	TA
Karachentsev et al. (2009)	$M(< 0.96\text{Mpc})$	1.9 ± 0.2	Local Hubble flow measurement
van der Marel et al. (2012)	M_{vir}	4.93 ± 1.63	TA
van der Marel et al. (2012)	M_{vir}	3.17 ± 0.57	Bayesian analysis
Partridge et al. (2013)	M_{vir}	4.73 ± 1.03	TA & Λ corrections
Diaz et al. (2014)	M_{vir}	2.4 ± 0.8	Momentum balance at the LG center of mass
González et al. (2014)	M_{200}	$2.40^{+0.55}_{-0.36}$	Likelihood estimate
González et al. (2014)	$M(< 1\text{Mpc})$	$4.17^{+1.45}_{-0.93}$	Likelihood estimate
Peñarrubia et al. (2016)	M_{vir}	$2.64^{+0.42}_{-0.38}$	TA & Large Magellanic Clouds corrections
McLeod et al. (2016)	M_{vir}	$4.9^{+0.8+1.3}_{-0.8-1.4}$	Machine learning & $v_{\text{tan}}^{(I)}$
McLeod et al. (2016)	M_{vir}	$3.6^{+1.3+1.7}_{-1.1-1.5}$	Machine learning & $v_{\text{tan}}^{(II)}$
Present paper	M_{200}	$1.79^{+0.51}_{-0.51}$	CS & $v_{\text{tan}}^{(I)}$
Present paper	M_{200}	$3.47^{+1.16}_{-0.83}$	CS & $v_{\text{tan}}^{(II)}$